Poly(vinylcaprolactam)-Based Biodegradable Multiresponsive Microgels for Drug Delivery

ARTICLE *in* BIOMACROMOLECULES · AUGUST 2013

Impact Factor: 5.75 · DOI: 10.1021/bm401131w · Source: PubMed

5 AUTHORS, INCLUDING:

Wuli Yang
Fudan University
154 PUBLICATIONS **4,703** CITATIONS

SEE PROFILE

Article

pubs.acs.org/Biomac

Poly(vinylcaprolactam)-Based Biodegradable Multiresponsive Microgels for Drug Delivery

Yang Wang,[†] Jinshan Nie,[‡] Baisong Chang,[†] Yangfei Sun,[§] and Wuli Yang*,[†]

[†]State Key Laboratory of Molecular Engineering of Polymers and Department of Macromolecular Science, Fudan University, Shanghai 200433, P. R. China

[‡]Department of Gastroenterology, Taicang No.1 People Hospital, the Affiliated Hospital of Soochow University, Taicang 215400, Jiangsu Province, P.R. China

[§]State Key Laboratory of Genetic Engineering and School of Life Sciences, Fudan University, Shanghai, 200433, China

Supporting Information

ABSTRACT: Poly(vinylcaprolactam) (PVCL)-based biodegradable microgels were prepared for the biomedical application as drug delivery system via precipitation polymerization, where *N*,*N*-bis(acryloyl) cystamine (BAC) served as cross-linker, methacrylic acid (MAA) and polyethylene glycol (PEG) methyl ether methacrylate acted as comonomers. The microgels with excellent stability had distinct temperature sensitivity as largely observed in the case of PVCL-based particles and their volume phase transition temperature (VPTT) shifted to higher temperature with increasing MAA content and ambient pH. In the presence of reducing agent glutathione (GSH) or dithiothreitol (DTT), the microgels could be degraded into individual linear polymer chains by the cleavage of the disulfide linkages coming from the cross-linker BAC. The microgels could effectively encapsulate Doxorubicin (DOX) inside and presented stimuli-triggered drug release in acidic or reducing environment. The results of the cytotoxicity assays further demonstrated that the blank microgels were nontoxic to normal cells while DOX-loaded microgels presented efficient antitumor activity to HeLa cells.

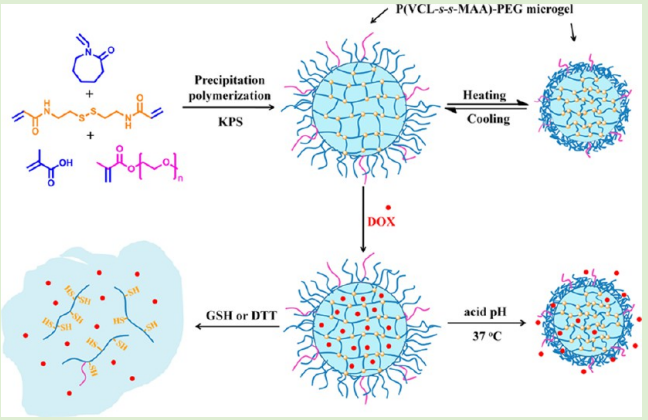

INTRODUCTION

Nanoparticles have been developed to enhance therapeutic efficacy and minimal side effect due to their enhanced permeability and retention (EPR) effect.[1−4] Among various dedicated nanoparticles for drug delivery applications, the burgeoning interest in polymer microgels has been greatly spurred since they exhibit more flexible and robust properties, including superior colloid stability, fluid-like transport properties, and fine control over particle size.[5,6] Moreover, the convenient functionalization of stimuli-responsive characters into microgels has gained increasing attention, which consequently results in readily controlled drug release by wielding an appropriate stimulus after arrival at the target site.[7−11] Although polymer microgels have validated great potential in delivering drugs, this technique is facing tremendous challenges. Many stimuli-responsive micogels failed to achieve optimal drug availability inside cancer cells because they were nondegradable, and thus insufficient intracellular drug was available for killing cancer cells.

Extensive attention has been focused on the microgels based on temperature-sensitive polymers because of their potential use for biomedical application.[12−16] Poly(*N*-isopropylacrylamide) (PNIPAM) microgel is a classical thermo-responsive material as controlled drug delivery systems, because it possesses a sharp phase transition and a volume phase transition temperature (VPTT) that is close to body temperature.[17,18] However, the potential utility of PNIPAM-based microgels was limited because of the unwanted neurotoxin.[19] To tackle this issue, one reliable strategy is to fabricate environment responsive and more biocompatible microgels. Poly(*N*-vinylcaprolactam) (PVCL) microgel has been proved to be an excellent drug carrier to trigger the release of embedded active compounds due to the temperature-dependent volume phase transition and the corresponding change in mesh sizes of the gel network.[19,20] As the polymer microgels cross-linked with noncleavable units partially block the diffusion of embedded drugs in-and-out of the carriers, some smart environmental triggers, such as pH, redox potential, light, or enzymes, can induce complete or partial cleavage of cross-linking points, resulting in the stimuli-triggered drug release for optimal drug availability.[6,21−23] In addition to pH changes throughout the body, another relevant biological trigger is the difference in the redox potential between the intracellular and extracellular compartments. The concentration of reducing glutathione (GSH) in the cytosol was approximately 2−10 mM,

Received: April 22, 2013
Published: August 2, 2013

Scheme 1. Illustration of the Preparation, Biodegradable Behavior and Stimuli-Responsive Drug Release of PVCL-Based Microgels

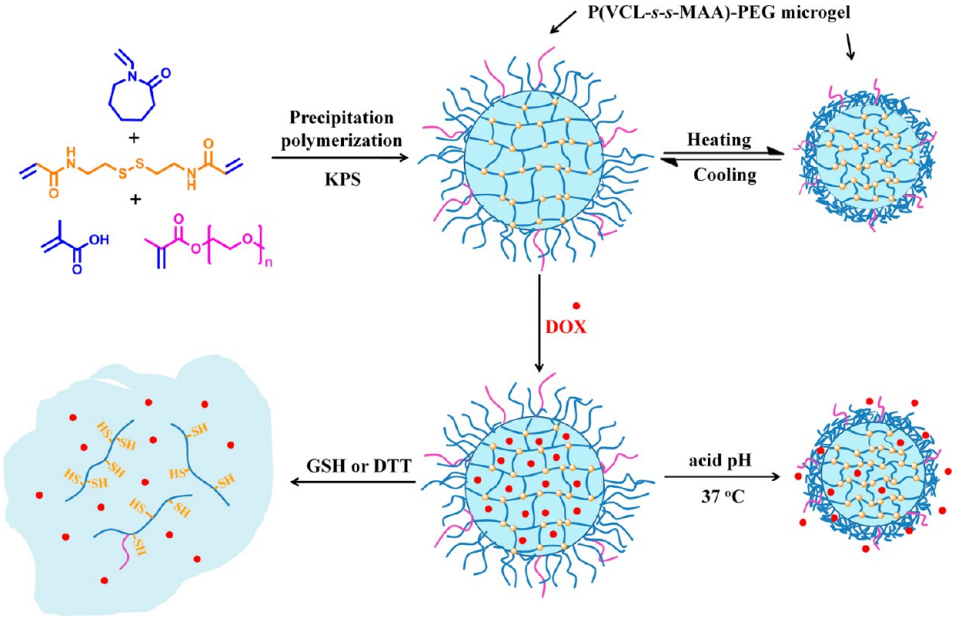

much higher than that in the extracellular fluids (approximately 2−20 μM).[24,25] Therefore, delivery vehicles based on disulfide-functionalized linkages cleavable in reductive condition received particular interest for intracellular drug delivery.[26] Matyjaszewski and co-workers reported the preparation of well-defined redox-responsive functional microgels using inverse mini-emulsion atom transfer radical polymerization and the disulfide-thiol exchange reaction.[6] Groll and his co-workers described the preparation of biocompatible and degradable microgels by cross-linking thiol-functionalized star-shaped poly(ethylene oxide-co-propylene oxide) and linear polyglycidol in inverse mini-emulsion.[27] These preparation procedures are relatively complicated and include several steps, which may prove restrictive to future applications. Therefore, the design of a delivery system with a simpler preparation is still of paramount importance.

Herein, we prepared the PVCL-based microgels using convenient and environmentally friendly precipitation polymerization method by incorporation of the disulfide-bonded cross-linker *N*,*N*′-bis(acryloyl)cystamine (BAC) to obtain a biocompatible, degradable, robust, and smart drug carrier that can release anticancer drugs in response to temperature, pH, and redox potential (Scheme 1). In our architecture, the smart microgels comprised an interior BAC-cross-linked polymer network formed by temperature-sensitive PVCL and pH-sensitive poly(methacrylic acid), and a polyethylene glycol (PEG)-rich corona to stabilize the particles. The microgels, stable in physiological condition, underwent adjustable VPTT with changing pH and methacrylic acid (MAA) mass and eroded quickly in reductive condition due to the cleavage of the disulfide linkages. Besides, the microgels could effectively encapsulate Doxorubicin (DOX) inside with high drug load content, and quickly release DOX when in acidic or redox environment.

EXPERIMENTAL SECTION

Materials. *N*-vinylcaprolactam (VCL, 99%) and PEG methyl ether methacrylate (PEGMA, M_w 2080, 50 wt % solution in water) were obtained from Sigma-Aldrich. *N*,*N*′-bis (acryloyl) cystamine (BAC) and *N*,*N*′-methylenebisacrylamide (MBA) were purchased from Fluka and used as received. 2-Aminoethyl methacrylate hydrochloride, L-dithiothreitol (DTT) and glutathione (GSH) were purchased from Shanghai Aladdin Chemistry Co. Ltd. Methacrylic acid (MAA), potassium persulfate (KPS), sodium dodecyl sulfate (SDS), and sodium bicarbonate ($NaHCO_3$) were obtained from Shanghai Chemical Reagents Company. Fluorescein isothiocyanate (FITC) and Doxorubicin (DOX) in the form of the hydrochloride salt was obtained from Beijing Huafeng United Technology Company. MAA was distilled under reduced pressure, and KPS was recrystallized twice from water prior to use. 3-(4,5-dimethylthiazol-2-yl)-2,5-diphenyltetrazolium bromide (MTT) and other biological reagents were purchased from Sigma Corp. The other chemicals were of analytical grade and were used as received.

Characterization. ^{1}H NMR was performed on a Bruker 400 MHz spectrometer using D_2O as solvent. Fourier transform infrared (FTIR) spectra were obtained on a Nicolet Nexus-440 FT-IR spectrometer. Raman spectra were obtained on LabRam-1B confocal microscopic Raman spectrometer. Transmission electron microscopy (TEM) images were obtained on a Hitachi H-600 transmission electron microscope, and the microgels were negative stained with 1% phosphotungstic acid for TEM measurement. UV−vis spectra were obtained using a Perkin-Elmer Lambda 35 spectrophotometer. Hydrodynamic diameter, zeta potential and light scattering intensity of the microgels were measured by using a dynamic light scattering (DLS) particle size analyzer (Malvern Nano-ZS90) at scattering angle of 90°. The average molecular weight and molecular weight distribution (M_w/M_n) of degradable polymer linear chains were estimated by gel permeation chromatography (GPC) measurements, which were carried out on a HP Angilent series 1100 Chromatograph equipped with a G1310A pump, a G1362A refractive index detector, and a G1315A diode-array detector. Poly(ethylene oxide) (PEO) standard samples were used for calibration, and the measurement condition is 0.1 M $NaNO_3$ aqueous solution at 40 °C with an elution rate of 0.5 mL/min. Intracellular tracking were subjected to observe with a confocal laser scanning microscope (CLSM) (Leica, TCS SP2). The fluorescence images were obtained on a fluorescence microscope (Olympus IX71, Tokyo, Japan).

Preparation of Microgels. Two families of microgels were synthesized by precipitation polymerization using a 150 mL glass flask as the reactor under nitrogen atmosphere. In the synthesis of P(VCL-*s*-*s*-MAA) microgels, 1 wt % of the sum (VCL + MAA) but different mass ratios of VCL to MAA (VCL/MAA: 100/0, 99/1, 98/2, 97/3, 96/4)

dx.doi.org/10.1021/bm401131w | *Biomacromolecules* 2013, 14, 3034−3046

were used (Table 1). Briefly, 1.00 g of VCL and MAA, 20.0 mg (2 wt %) of SDS, 25.0 mg (2.5 wt %) of $NaHCO_3$, and 40.0 mg (4 wt %) of BAC

Table 1. The Recipes and Colloidal Data of Microgels

sample	VCL (mg)	MAA (mg)	D_h[c] (nm)	PI[d]
P(VCL-*s*-*s*-MAA-0[a])	1000	0	125	0.04
P(VCL-*s*-*s*-MAA-1)	990	10	135	0.07
P(VCL-*s*-*s*-MAA-2)	980	20	177	0.07
P(VCL-*s*-*s*-MAA-3)	970	30	237	0.08
P(VCL-*s*-*s*-MAA-4)	960	40	281	0.06
P(VCL-*s*-*s*-MAA-3)-PEG[b]	970	30	202	0.04

[a]Weight ratio of MAA in respect to sum of MAA and VCL. [b]10 mg of PEGMA was used in the recipe. [c]The hydrodynamic diameter (D_h) was determined in phosphate buffer of 7.4 at 25 °C by DLS. [d]PI, polydispersity index of the particle size,[30] PI = $\langle\mu_2\rangle/\Gamma^2$.

dissolved in 100 g water was prepared in a three-neck flask equipped with a reflux condenser, then the reactor contents were heated to 70 °C and kept under nitrogen atmosphere. After mechanical stirring of 200 rpm for 0.5 h, 25 mg KPS (2.5 wt % to the monomers) dissolved in 2 mL distilled water was rapidly added, and the mixture immediately became turbid. The polymerization reaction was allowed to continue under nitrogen atmosphere with stirring for 6 h. The reaction mixture was subsequently cooled to 25 °C, while maintaining the stirring and nitrogen flow to prevent possible aggregation. Finally, the obtained microgels were dialyzed for a week via a dialysis bag (molecular weight cut off 14000) to remove the unreacted reagents and impurities. In the synthesis of P(VCL-*s*-*s*-MAA)-PEG microgels, VCL, MAA, $NaHCO_3$, SDS, and BAC were dissolved in the reactor at the beginning of the reaction, then a shot of 10.0 mg of PEGMA (1 wt % in respect to the sum of MAA and VCL) was added into the reaction mixture after 30 min of polymerization for the formation of PEGMA-rich corona. Likewise, the linear copolymer P(VCL-*co*-MAA) and the microgels cross-linked with MBA containing the same amount of MAA and PEGMA as P(VCL-*s*-*s*-MAA)-PEG microgels were prepared for comparison.

Thermo/pH-Sensitivity of Microgels. The thermo/pH-sensitive behavior of the microgels was investigated by DLS measurement. The temperature-sensitivity of the microgels was analyzed by monitoring the change of hydrodynamic diameters as a function of pH or MAA content with increasing temperature from 20 to 65 °C. Likewise, the pH-sensitivity of the microgels was investigated by tracing the hydrodynamic diameters and zeta potential of the microgels as a function of MAA contents in phosphate buffers of different pH at 25 °C. All the microgels were measured at a concentration of 1.0 mg mL^{-1}.

Stability of Microgels. To evaluate the stability of P(VCL-*s*-*s*-MAA)-PEG microgels, the hydrodynamic diameter and size distribution were measured in PBS 7.4 at different concentrations of salt (0 M, 0.5 M, 1M, 2M). The microgels were measured at the concentration of 1.0 mg mL^{-1} at 25 °C.

Redox Response of Disulfide-Bonded Microgels. The reducing degradation of P(VCL-*s*-*s*-MAA)-PEG microgels was conducted by tracing the turbidity and hydrodynamic diameter change of the microgels in responsive to different concentrations of reducing agents (DTT or GSH). Samples with an identical particle concentration of 1.0 mg mL^{-1} were prepared in pH 7.4 phosphate buffers containing 0, 10, 20, 40 mM GSH or 0, 1, 5, 10 mM DTT. Subsequently, the prepared samples were allowed to be incubated in water bath at 37 °C for erosion, and the scattering light intensities at 90° and the average hydrodynamic diameters of samples were measured by using DLS at predetermined intervals. The ratio of the scattering intensity of microgels at a predetermined interval to that of the initial nondegraded microgels was calculated to determine the relative turbidity. To avoid M_w influence from PEGMA, P(VCL-*s*-*s*-MAA) microgels at the concentration of 1.0 mg mL^{-1} were incubated for 24 h in the pH 7.4 phosphate buffers with 40 mM GSH or 10 mM DTT at 37 °C for adequate degradation. The obtained degraded polymer solutions were collected and the molecular weight of the degraded polymers was measured in 0.1 M $NaNO_3$ aqueous solution by GPC after the polymer solutions were filtered through 0.45 μm filter without strong pressing prior to its injection into the GPC.

DOX Loading and Release. DOX was chosen as a model drug to investigate the drug loading and controlled release behavior of microgels. Briefly, 10 mg of P(VCL-*s*-*s*-MAA)-PEG microgels was dispersed into 3 mL of DOX aqueous solution (1 mg/mL) adjusted to pH 8.0. After gentle stirring for 24 h at room temperature, the dispersion was centrifuged to collect the DOX-loaded microgels and then washed with distilled water twice to remove the surface adsorption of DOX. The DOX content in the supernatant was determined by UV−vis spectrometry at 480 nm against the established calibration curve. The drug loading content and encapsulation efficiency were calculated using formulas 1 and 2 respectively:

$$\text{Loading content (\%)} = \frac{\text{mass of drug in microgels}}{\text{mass of drug-loaded microgels}} \quad (1)$$

$$\text{Encapsulation efficiency (\%)} = \frac{\text{Initial mass of drug} - \text{mass of drug in supernatant}}{\text{Initial mass of drug}} \quad (2)$$

In vitro release study was performed in a glass apparatus at 37 °C in four different phosphate buffers with 150 mM NaCl (pH 7.4, 6.5, 5.5, and pH 6.5 + 10 mM GSH). Typically, 1 mg of DOX-loaded P(VCL-*s*-*s*-MAA)-PEG microgels was dispersed in 1 mL corresponding buffer and then placed into a dialysis bag, which was subsequently immersed in 100 mL of the release medium and gently shaken at 37 °C to acquire sink conditions. At timed intervals, 2 mL of external buffer was withdrawn from the reservoir and analyzed by UV−vis absorption, and then 2 mL of the fresh buffer was added to keep the volume of the release medium invariable. All measurements were performed in triplicate, and the releasing content was calculated by formula 3:

$$\text{Releasing content (\%)} = \frac{\text{amount of drug in the release medium}}{\text{amount of drug loaded into microgels}} \quad (3)$$

In Vitro Cell Assays. HK-2 cells (human tubular epithelial cells, normal cells) and HeLa cells (human cervical carcinoma cells, cancer cells) were cultured in Dulbecco's modified Eagle's medium (DMEM) supplemented with 10% FBS (fetal bovine serum), penicillin (100 U/mL) and streptomycin (100 mg/mL) in a humidified atmosphere with 5% CO_2 at 37 °C.

To observe the uptake of the P(VCL-*s*-*s*-MAA-3)-PEG microgels by HeLa cells, FITC was conjugated into the microgels by copolymerization of FITC-functionalized monomer. FITC was conjugated with 2-aminoethyl methacrylate to form FITC-functionalized monomer. FITC (4.1 mg) and 1.6 mg of 2-aminoethyl methacrylate were dissolved in 2 mL of dimethyl sulfoxide (DMSO), then 10 μL triethylamine was added into the solution. The mixture was stirred with a magnetic stirrer for 12 h at 25 °C. The above reaction mixture and the requisite PEGMA aqueous solution were added simultaneously into the polymerization system after 30 min of polymerization. To investigate the effectiveness of the microgels as drug carriers, HeLa cells were treated with FITC-labeled blank microgels for 0.5 h, 1 h, 2 and 4 h, respectively. Then cells were washed with PBS (pH 7.4) three times. The intracellular distribution of the microgels was observed by CLSM.

Fluorescence images of the cells were taken with blue excitation to investigate the intracellular DOX release from the microgels. HeLa cells were cultured at a density of 1×10^4 cells/well and incubated in six-well plates with the DOX-loaded microgels on the final DOX concentration of 0.1 μg mL^{-1}. At timed intervals (2, 8, 24, and 48 h), fresh DMEM and PBS were added to wash off the free microgels not phagocytized by cells before fluorescence observation. Free DOX (0.1 μg mL^{-1}) was treated under the same conditions for 24 and 48 h, respectively.

The cytotoxicity assay of DOX-loaded and blank microgels against HeLa cells were assessed by the standard MTT assay. Typically, HeLa cells were seeded at a density of 8×10^3 cells/well and incubated in 96-well plates for 24 h to allow cell attachment. Then the cells were treated with blank microgels, DOX-loaded microgels, and free DOX at various

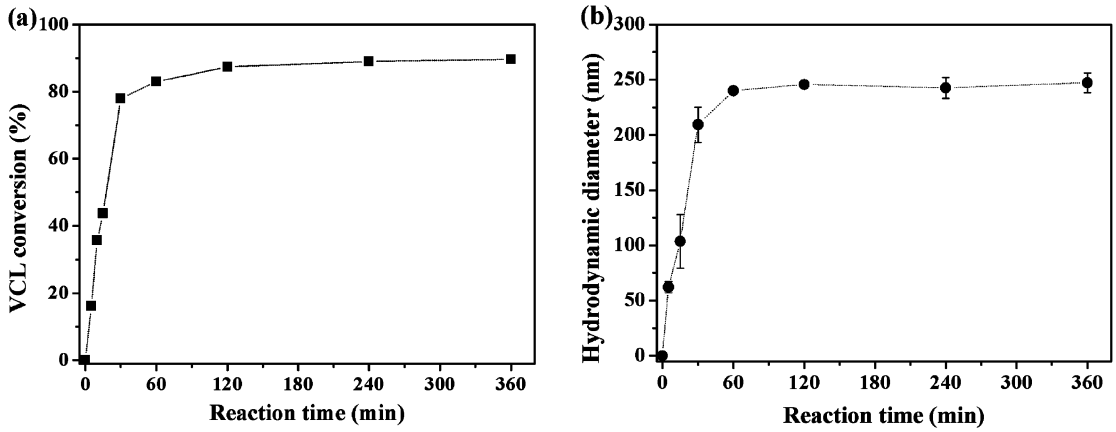

Figure 1. Evolution of the conversion of VCL (a) and the hydrodynamic diameter of the P(VCL-*s*-*s*-MAA-3) microgels during the polymerization (b).

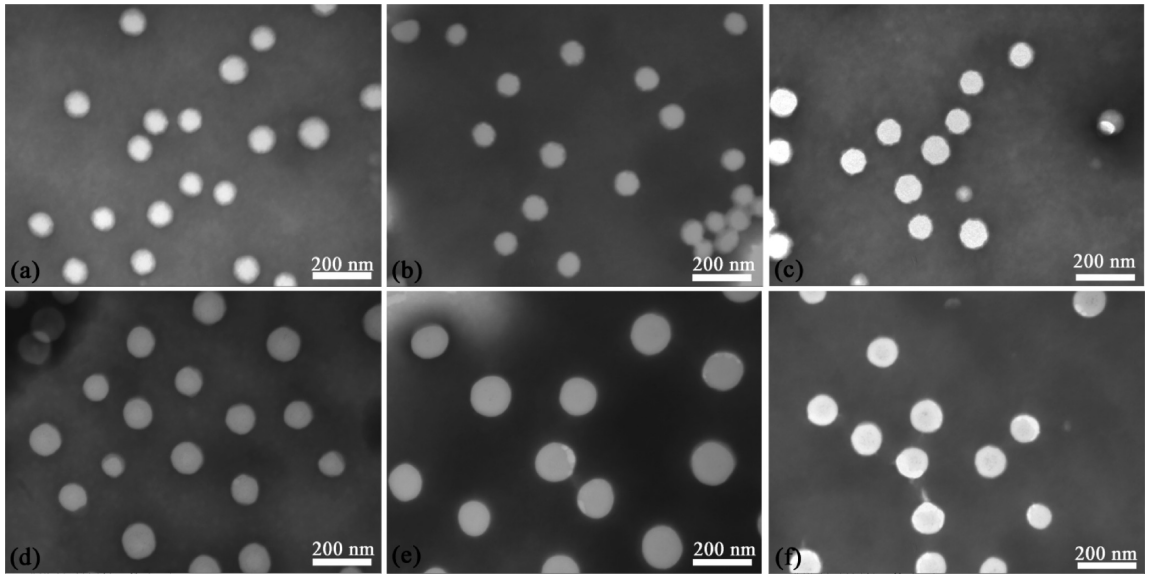

Figure 2. TEM images of P(VCL-*s*-*s*-MAA) microgels. (a) 0 wt % MAA, (b) 1 wt % MAA, (c) 2 wt % MAA, (d) 3 wt % MAA, (e) 4 wt % MAA, and (f) P(VCL-*s*-*s*-MAA-3)-PEG microgels.

concentrations and incubated for 48 h at 37 °C. Next, 20 μL of MTT solution (5 mg mL^{-1} in PBS) was replaced with fresh DMEM containing MTT (5 mg mL^{-1}), and the cells were incubated for another 4 h. Then, the supernatant was removed, and 150 μL of DMSO was added to each well to dissolve the formazan. The absorbance was monitored at 570 nm using a spectrophotometer after 10 min of incubation. Each data point was collected by averaging that of three wells, and the untreated cells were used as controls. Percentage cell viability was calculated by comparing the absorbance of the control cells to that of treated cells. The same process of cytotoxicity of blank microgels against HK-2 cells was performed as mentioned above.

RESULTS AND DISCUSSION

Preparation of PVCL-Based Microgels. Precipitation polymerization is a common technique for the preparation of water-swellable thermo-sensitive microgels.[17] As no, or minimal surfactants are utilized in precipitation polymerization, the problem of residual surfactant contamination can be resolved easily. Besides, precipitation polymerization is a simpler one-pot preparation method for synthesis of microgels. During precipitation polymerization, the growing polymer chains collapse when they reach a critical length and form particle nuclei due to the phase-separate from the continuous medium by enthalpic precipitation above its LCST.[28] Afterward, the resulting nuclei further aggregate to form large colloidally stable polymer particles (microgels) which can be stabilized by the charges originating from the initiator fragments (sulfate groups) incorporated into polymer chains. The prepared microgel aqueous dispersion was a swelling network at room temperature and could remain stable by steric mechanisms due to the formation of hydrogen bonds between polymer segments and water molecules. In this work, a new type of PVCL-based network was prepared with VCL, MAA, PEGMA, and the disulfide-bonded cross-linker BAC in precipitation polymerization (Scheme 1 and Table 1). KPS was used as initiator, and $NaHCO_3$ acted as buffer to avoid hydrolysis of VCL.[29] The incorporation of pH-sensitive monomer MAA and hydrophilic macromonomer PEGMA enhanced the microgel stability by electrostatic and steric mechanisms.

To investigate the conversion of the monomers, the P(VCL-*s*-*s*-MAA-3) microgel was prepared in deuterium oxide, and the products at different reaction time were analyzed by ^{1}H NMR. The signal at 7.1 ppm was assigned to the proton of −CH═ group, and the signals at 4.6 and 4.8 ppm corresponded to the two protons of the allyl group (CH_2═) in the ^{1}H NMR

dx.doi.org/10.1021/bm401131w | *Biomacromolecules* 2013, 14, 3034−3046

spectrum of VCL (Figure S1, Supporting Information). The signal at 7.1 ppm corresponding to the proton of −CH═ group got weaker with increased time, and was very feeble after 120 min of polymerization. As MAA and BAC presented very weak signals in ^{1}H NMR due to the low concentration, it was difficult to accurately analyze their conversions. Thus, we analyzed the conversion of main monomer VCL based on the integral change of the peaks at 7.1 ppm at different intervals. Figure 1a shows that the conversion of main monomer VCL increased with time extending, and about 80% of VCL had been respectively consumed after 30 min of polymerization, which suggested the addition of PEGMA after 30 min of polymerization facilitated the formation of PEGMA-rich corona. Meanwhile, we monitored the evolution of the hydrodynamic diameter of the microgels in the reactions by DLS (Figure 1b), and the size of the microgels increased to about 210 nm after 30 min of polymerization, close to the final size.

The average hydrodynamic diameter of the microgels increased from 125 to 281 nm with narrow size distribution (PI < 0.1)[30] upon increasing the amount of MAA in the recipe from 0 to 4 wt % (Table 1). The reproducibility of the batches is good (Table S1). More hydrophilic MAA incorporated into the polymer network made the microgels more swollen, leading to the larger size.[31] Figure 2a to 2e showed the TEM images of P(VCL-*s*-*s*-MAA) microgels with different MAA content. All the microgels exhibited uniform and regular spherical morphology. The size of the microgels observed in TEM increased from 86 ± 15 nm (0 wt % MAA) to 138 ± 10 nm (4 wt % MAA), which was in accord with the DLS order (Table 1). As MAA weight fraction increased, the growing polymer chains during precipitation polymerization became more hydrophilic and were unable to undergo efficient chain collapse, therefore, the particle nuclei number was decreased, resulting in a larger size.[32]

In contrast with the size measured by DLS, the size determined by TEM was much smaller, which was due to the swollen state for DLS measurement and the collapsed state for TEM observation. This meant the microgels have obvious swelling/deswelling behavior. For the P(VCL-*s*-*s*-MAA-3) microgels, the size in the swollen state and shrunk state was 237 and 113 nm, respectively. Therefore, the swelling ratio of the P(VCL-*s*-*s*-MAA-3) microgels was determined to be 2.10 by calculating the ratio of the size in the swollen state and shrunk state. According to the model describing the correlation between swelling ratio and cross-link density (mol %) proposed by Varga,[33] the cross-link density could be calculated to be 2.98 mol %, close to the theoretic cross-link density (2.2 mol %). The TEM image of the P(VCL-*s*-*s*-MAA-3)-PEG microgels was illustrated in Figure 2f. The microgels presented regular global shape and scattered homogeneously, which was consistent with the DLS results (PI, 0.04). The TEM size was 110 ± 15 nm, slightly smaller than that of P(VCL-*s*-*s*-MAA-3) microgels (113 ± 15 nm, Figure 2d). As mentioned above, since the size measured by DLS is much larger than that measured by TEM, the difference in size measured by TEM between P(VCL-*s*-*s*-MAA-3) and P(VCL-*s*-*s*-MAA-3)-PEG microgels was much smaller. On the other hand, the average hydrodynamic diameter measured by DLS had statistical significance, and the size was measured by TEM based on the finite number of particles shown in TEM images. Therefore, compared with the difference in the size measured by DLS between P(VCL-*s*-*s*-MAA-3) and P(VCL-*s*-*s*-MAA-3)-PEG, the difference in the TEM size was much smaller.

The chemical structures of P(VCL-*s*-*s*-MAA) and P(VCL-*s*-*s*-MAA)-PEG microgels were characterized by FTIR spectroscopy (Figure 3). The peaks appearing at 1630 cm^{-1} and 1481 cm^{-1} were attributed to the amide I band, and C−N belonged to the

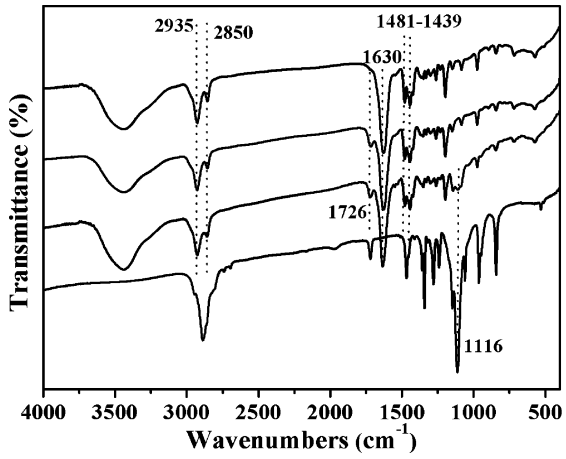

Figure 3. FTIR spectra of P(VCL-*s*-*s*-MAA-0), P(VCL-*s*-*s*-MAA-3), P(VCL-*s*-*s*-MAA-3)-PEG, and PEGMA (from up to down).

characteristic peaks of PVCL.[13] The bands appearing at 2935, 2850, and 1439 cm^{-1} were attributed to stretching and bending vibrations of C−H groups, respectively.[34] In the spectra of P(VCL-*s*-*s*-MAA-3) and P(VCL-*s*-*s*-MAA-3)-PEG, the peak at 1726 cm^{-1} was attributed to the stretching vibration of C═O originating from PMAA,[13] which indicated that MAA had been incorporated into the microgels successfully. In the spectra of P(VCL-*s*-*s*-MAA-3)-PEG and PEGMA, the typical absorption band of ether coming from PEGMA macromonomer was found at 1116 cm^{-1},[35] indicating that PEGMA macromonomer had been successfully copolymerized into the microgels. The existence of disulfide bonds in the polymer network was confirmed by comparing the Raman spectrum of the BAC-cross-linked microgel with that of the microgel cross-linked with MBA (a cross-linker without disulfide bonds). As illustrated in Figure 4, the clearly visible peak at 510 cm^{-1} in the spectrum of

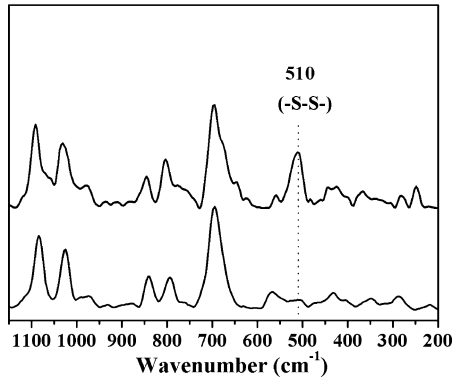

Figure 4. Raman spectra of microgels cross-linked with BAC (up) and MBA (down).

the BAC-cross-linked microgels was attributed to the vibration of disulfide bond (S−S),[36] demonstrating that disulfide bonds were successfully introduced into the microgels via copolymerization with cross-linker BAC.

Thermo/pH-Sensitivity of Microgels. The temperature-sensitivity of the P(VCL-*s*-*s*-MAA) microgels at pH 6.5 is shown in Figure 5a. All the prepared microgels containing 1 to 4 wt %

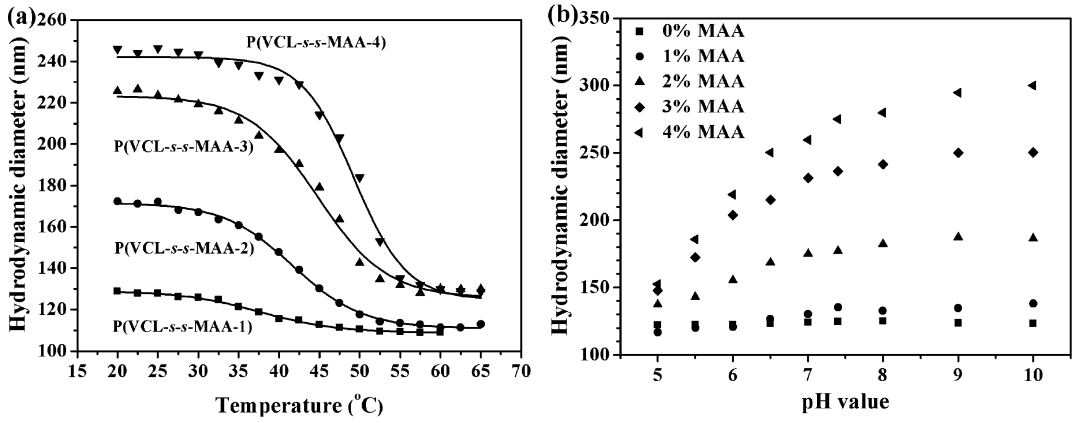

Figure 5. Effect of MAA content on the temperature dependence of the hydrodynamic diameter in phosphate buffer of pH 6.5 (a) and on the pH dependence of the hydrodynamic diameter of P(VCL-*s*-*s*-MAA) microgels at 25 °C (b).

Table 2. Thermo/pH-Sensitivity of P(VCL-*s*-*s*-MAA) and P(VCL-*s*-*s*-MAA-3)-PEG Microgels

	zeta potential[a]						
sample	5.5	6.5	7.4	$VPTT_{5.5}$ (°C)	$VPTT_{6.5}$ (°C)	$VPTT_{7.4}$ (°C)	VPTT[b] (°C)
P(VCL-*s*-*s*-MAA-0)	−0.8	−1.6	−2.5	/	/	/	/
P(VCL-*s*-*s*-MAA-1)	−3.5	−5.2	−6.7	/	37.4	43.6	/
P(VCL-*s*-*s*-MAA-2)	−6.9	−8.9	−11.5	/	41.8	45.9	37.6
P(VCL-*s*-*s*-MAA-3)	−8.4	−15.6	−17.0	28.5	44.0	47.5	40.0
P(VCL-*s*-*s*-MAA-4)	−9.1	−17.4	−20.4	29.0	49.1	N/A	44.2
P(VCL-*s*-*s*-MAA-3)-PEG	−8.9	−16.0	−18.4	29.5	45.2	48.2	41.0

[a]The zeta potential was determined in phosphate buffers of different pH at 25 °C. [b]The VPTT was determined in phosphate buffer of pH 7.4 with 0.15 M NaCl.

MAA shrank upon increasing the temperature as largely observed in the case of PVCL-based particles.[37] The hydrodynamic diameter of P(VCL-*s*-*s*-MAA-3) microgels decreased from 226 nm at 20 °C to 130 nm at 65 °C. It was obviously observed that P(VCL-*s*-*s*-MAA) microgels with higher MAA content underwent volume phase transition at significantly higher temperatures than those with lower MAA content. At pH 6.5, the VPTT of the P(VCL-*s*-*s*-MAA-1) microgels was 37.4 °C, while that of the P(VCL-*s*-*s*-MAA-4) microgels shifted to 49.1 °C (Table 2). Similarly, at pH 7.4, the VPTT of P(VCL-*s*-*s*-MAA-1) microgels was 43.6 °C, while the collapse of P(VCL-*s*-*s*-MAA-4) microgels was almost fully retarded without significant volume phase transition observed. It was found in Table 2 that no clear VPTT was observed in P(VCL-*s*-*s*-MAA-0) microgels as the stability of particles was destroyed by the increased temperature due to the enhancement of hydrophobic interactions among the PVCL chains.[38] The hydrophilicity and electrostatic repulsion of polymer segments increased when MAA contents increased, thus the balance of repulsive and hydrophobic force would be broken at higher incubation temperature, which resulted in a higher VPTT.[39]

Figure 5b reflects the dependence of hydrodynamic diameter for P(VCL-*s*-*s*-MAA) microgels as a function of pH (from 5.0 to 10.0) and MAA content at 25 °C. The hydrodynamic diameter of all the P(VCL-*s*-*s*-MAA) microgels was capable of much larger swelling from pH 5.0, which corresponded to the increase of electrostatic repulsion force in higher pH. As pH increased from 5.5 to 7.4, the hydrodynamic diameter of the P(VCL-*s*-*s*-MAA-3) microgels rose from 172 to 236 nm, corresponding to the zeta potential changing from −8.4 to-17.0 mV (Table 2). The increased charge density in basic environment arising from ionization of carboxyl groups should lead to a larger size due to the electrostatic repulsion force.[40] In addition, the P(VCL-*s*-*s*-MAA) microgels exhibited greater swelling behavior with more incorporation of MAA in recipe. For example, the size of P(VCL-*s*-*s*-MAA-4) microgels increased from 152 nm at pH 5.0 to 300 nm at pH 10.0, while that of the P(VCL-*s*-*s*-MAA-0) microgels remained variable. As for constant pH condition, especially in basic environment, the hydrodynamic diameter of the microgels showed increased swelling with increasing MAA content. The size rose from 125 to 281 nm at pH 7.4 as MAA mass ratio increased from 0 wt % to 4 wt % (Table 1), which was associated with the result that the zeta potential of the microgels became more negative as MAA mass fraction increased (Table 2). At pH 7.4, the zeta potentials changed from −2.5 mV for P(VCL-*s*-*s*-MAA-0) microgels to −20.4 mV for P(VCL-*s*-*s*-MAA-4) microgels. More MAA increased negative charge density on the microgel surface due to the complete ionization of the carboxyl groups from MAA in basic pH, which increased the electrostatic repulsion force, resulting in an increase of the microgel size.[41]

Since the microgels were pH sensitive due to the incorporation of MAA, the pH of the ambient medium should be one of the major factors that could regulate the thermosensitive properties of the microgels. The influence of pH on the temperature-sensitive behavior of the microgels was analyzed by investigating the hydrodynamic diameter of the microgels with the same amount of MAA as a function of temperature at different pHs. It can be noticed from Figure 6 and Table 2 that the P(VCL-*s*-*s*-MAA) microgels presented broader volume phase transition and higher VPTT with increasing ambient pH. In Figure 6, the protonated P(VCL-*s*-*s*-MAA-3) microgels at pH 5.5 displayed the sharpest volume phase transition and the lowest VPTT of 28.5 °C, while those ionized at 7.4 showed the broadest volume

dx.doi.org/10.1021/bm401131w | *Biomacromolecules* 2013, 14, 3034−3046

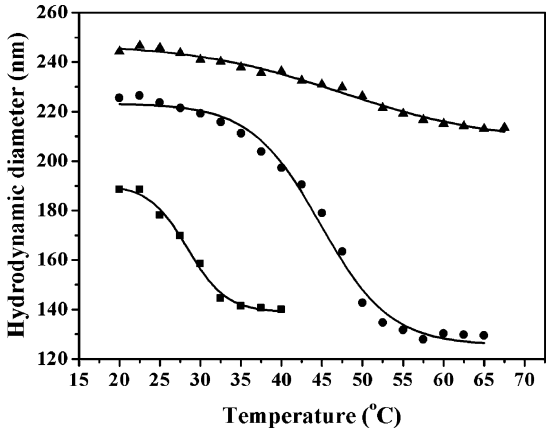

Figure 6. Effect of temperature on the hydrodynamic diameter of P(VCL-*s*-*s*-MAA-3) microgel in different pH condition (pH 5.5 (■), pH 6.5 (●), and 7.4(▲)).

phase transition and the highest VPTT of 47.5 °C. In Table 2, in acidic conditions of pH 5.5, the P(VCL-*s*-*s*-MAA) microgels with MAA content less than 3 wt % did not present VPTT with increasing temperature because they aggregated before reaching the VPTT due to the disappearance of the electrostatic stabilization provided by the ionized carboxylic groups.[42] These results were related to the increased negative charges originating from carboxyl groups of MAA in higher pH condition. As the negative carboxyl group of MAA completely ionized at higher pH (pK_a 4.9[40]), the noticeably increased negative charges on the particle surface increased the hydrophilicity and stability of microgels and weakened the swelling/deswelling behavior.

It can be seen in Table 2 that salinity affects the temperature-sensitivity of the microgels. In comparison to pH 7.4 without salt, the addition of salt made a lower VPTT. For P(VCL-*s*-*s*-MAA-3) microgels, the VPTT measured at pH 7.4 without salt was 47.8 °C, and shifted to 40.0 °C in pH 7.4 buffer with 0.15 M NaCl. The P(VCL-*s*-*s*-MAA-1) microgels underwent volume phase transition at 43.6 °C in NaCl-free solution of pH 7.4, while they were not stable during the rise in temperature with addition of 0.15 M NaCl, thus VPTT was not gotten. The addition of salt screened the negative charges from carboxyl groups and weakened the electrostatic repulsive forces between the anionic chain,[43] leading to the decrease of hydrophilicity and stability of the microgels. In this regard, the combination force of the electrostatic repulsion compensated by the hydrophobic force from PVCL chains was decreased due to the addition of NaCl, leading to a lower VPTT.[44]

Excellent thermosensitive microgels applicable in biomedicine as drug carriers should undergo a distinct transition around the human body environment: swollen state in bloodstream and collapsed state in tumor tissues, thus there is almost no premature drug release during blood circulation but rapid release upon reaching the tumor tissues. With this consideration, the VPTT of the P(VCL-*s*-*s*-MAA) microgels was investigated in analogic physiological conditions (pH 7.4 + 0.15 M NaCl). It can be observed in Table 2 that the P(VCL-*s*-*s*-MAA-3) microgels presented the VPTT of 40.0 °C, higher than and close to the physiological value of 37 °C. Therefore, PEGMA macromonomer was introduced into the P(VCL-*s*-*s*-MAA-3) network to improve the stability and biocompatibility of the synthetic microgel. As expected, the P(VCL-*s*-*s*-MAA-3)-PEG microgels remained the similar temperature sensitivity as the P(VCL-*s*-*s*-MAA-3) microgels. The VPTT measured in pH 7.4 with 0.15 M NaCl was 41.0 °C, 1 °C higher than that of P(VCL-*s*-*s*-MAA-3), which suggested that the incorporation of macromonomer PEGMA indeed increased the hydrophilicity and steric stability of the microgel as largely observed in the case of PEG-modified particles.[45] In this case, the swollen P(VCL-*s*-*s*-MAA-3)-PEG microgels at physiological temperature would not leak the drug in bloodstream due to the higher VPTT. The incorporation of PEGMA also could improve the stability of microgels with low MAA contents. Likewise, the P(VCL-*s*-*s*-MAA-3)-PEG presented the semblable pH sensitivity. As shown in Table 2, the zeta potential of the P(VCL-*s*-*s*-MAA-3)-PEG microgels changed from −8.9 mV to −18.4 mV with pH increasing from 5.5 to 7.4, the VPTT increased from 29.5 °C at pH 5.5 to 48.2 °C at pH 7.4. Figure 7 showed the stability of P(VCL-*s*-*s*-MAA-3)-PEG microgels against different concentrated salt conditions. The microgels remained structural integrity and excellent monodispersity even in the presence of 2 M NaCl. As shown in Table 3, the hydrodynamic diameter of the microgels decreased from 200 nm (0 M NaCl) to 168 nm (2 M NaCl). The addition of salt made the combination force of the electrostatic repulsion compensated by the hydrophobic force from PVCL chains decreased, leading to a smaller size. Owing to the excellent stability and the higher VPTT, the P(VCL-*s*-*s*-MAA-3)-PEG microgel shows great promise as a drug delivery vehicle for cancer therapy.

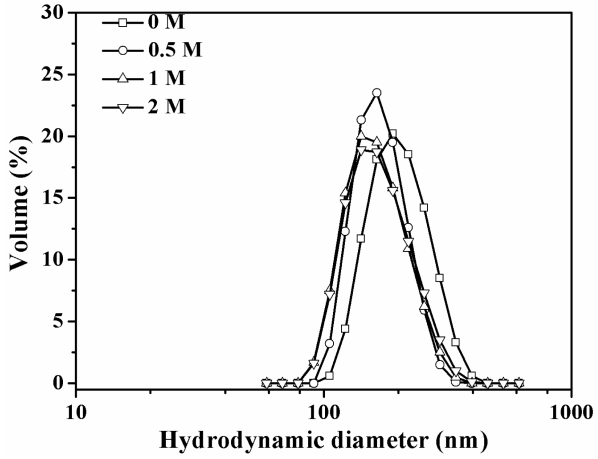

Figure 7. Stability against different NaCl concentrations of the P(VCL-*s*-*s*-MAA-3)-PEG microgels measured at 25 °C by DLS at an angle of 90° with a concentration of 1.0 mg mL^{-1}.

Table 3. The Colloidal Data of P(VCL-*s*-*s*-MAA-3)-PEG Microgels against Different NaCl Concentrations

NaCl concentration	D_h[a] (nm)	PI
0 M	200	0.04
0.5 M	180	0.03
1 M	172	0.03
2 M	168	0.01

[a]The measured hydrodynamic diameter was volume average diameter.

Redox Degradation of the Microgels. Successful incorporation of BAC within the microgel network should result in the degradation of the microgels via thiol-disulfide exchange reaction. The degraded polymer could be easily eliminated through the excretion pathway in vivo, resulting in reduced

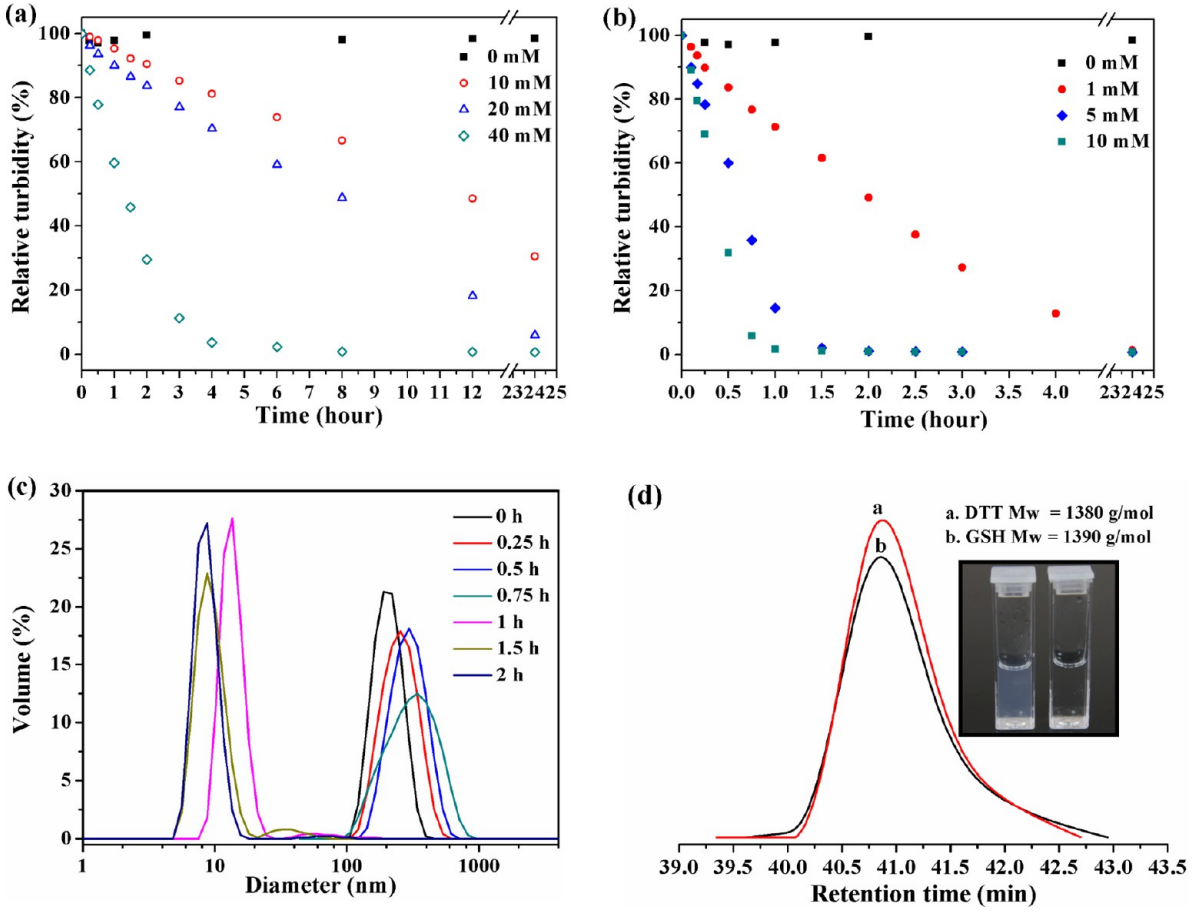

Figure 8. Investigations on the redox-induced microgel degradation: (a) The relative turbidity in the presence of different concentrations of GSH. (b) The relative turbidity in the presence of different concentrations of DTT; (c) The size change of the microgels in the presence of 10 mM DTT at pH 7.4 within 2 h; (d) Investigation on the microgel degradation by GPC measurement (the embedded photograph was the appearance of undegraded microgels (left) and degraded microgels (right)). The erosion behavior of microgels was analyzed by DLS with the concentration of 1.0 mg mL^{-1} at 37 °C.

cytotoxicity.[46] The DLS measurements by tracing the change of turbidity and size in response to reductive agents provided excellent insight into the redox degradation of the P(VCL-*s*-*s*-MAA-3)-PEG microgel.

In the turbidity measurement by DLS, the relative turbidity was determined to evaluate the degradation extent of the P(VCL-*s*-*s*-MAA-3)-PEG microgels by calculating the ratio of the scattering intensity of the microgels to that of the initial nondegraded microgels. DTT and GSH, widely used in disulfide-thiol reaction,[47] acted as reducing agents in our degradation experiments. Figure 8 shows the degradation extent of the microgel expressed as relative turbidity measured at pH 7.4 in the presence of different concentrations of reducing DTT or GSH. In the absence of GSH or DTT, the relative turbidity of the microgel was almost 100%, indicating no degradation. After 24 h of incubation in 10, 20, 40 mM GSH, the relative turbidity respectively decreased to 30.5%, 6.0% and 0.8%, which implied the higher concentration of reducing agents accelerated the erosion rate as more disulfide bonds were cleaved in higher concentration. It was noted that the microgels degraded more rapidly when exposed to reductive agent of DTT (Figure 8b). The relative turbidity of the microgels within 1 h declined to 32.0% when incubated in 10 mM DTT while it declined to 95.2% when the microgels were exposed to 10 mM GSH. This result was related to the reducing capacity which was determined by reduction potential. In pH 7.0 condition, the reduction potential of DTT was lower than that of the GSH.[25] DTT could revert to an internal oxidized disulfide bond and left behind a pair of thiols on the microgels. On the contrary, GSH likely reacted with BAC by participating in a single thiol-disulfide exchange reaction, resulting in a product with mixed-disulfide. Therefore, the possibility of reverse reactions and continued thiol-exchange reactions made the slower cross-link scission in the presence of GSH.[48]

To better demonstrate the redox-response, the P(VCL-*s*-*s*-MAA-3)-PEG microgels were treated with 10 mM DTT in phosphate buffer 7.4 at 37 °C, and at different timed intervals, the particle size and size distribution of the microgels were measured by DLS. Before degradation, the microgels had the mean size of 200 nm, and presented a uniform emulsion (Figure 8d, insert left). As shown in Figure 8c, the microgels swelled to 270 nm within 0.75 h, accompanied by the gradually increased PI (from 0.04 to 0.3) due to the decreased cross-linking density caused by the scission of the cross-linker. After degradation proceeded to 1 h, the hydrodynamic diameter of most microgels decreased to about 16 nm with small amounts of 60 nm microgels, which meant that the polymer network was disassembled into small polymer chains due to the cleavage of most disulfide bonds in the microgels. When proceeding to 2 h, all cross-linking points within the microgels were labile and complete dissolution of the microgel resulted in a small size of about 7 nm. As a consequence, the turbid dispersion turned into the corresponding transparent

dx.doi.org/10.1021/bm401131w | *Biomacromolecules* 2013, 14, 3034−3046

solution (Figure 8d, insert right). Albeit it is difficult for DLS to accurately measure such small size, the data could demonstrate that the particles turned smaller with increased time, indicating the degradation proceeded in the reducing medium.

GPC measurements were further used to analyze the molecular weight of the degraded polymer chains in the presence of GSH or DTT. To avoid M_w influence from PEGMA, The P(VCL-*s*-*s*-MAA-3) microgel was exposed to excess GSH or DTT for adequate degradation. The solution of degraded polymers could be filtered through a 0.45 μm-filter easily, prior to its injection to GPC, indicating the formation of degraded linear polymers. In Figure 8d, the GPC trace indicated that the degraded polymers had a low molecular weight (M_w, 1400 g/mol) and narrow molecular weight distribution (M_w/M_n, 1.1) in the presence of GSH or DTT. The cross-linking points in the microgel were cleaved through disulfide−thiol exchange reaction, leading to the formation of the short linear polymers with narrow molecular weight distribution. Linear copolymer P(VCL-*co*-MAA-3) was prepared by the same preparation procedure just without cross-linker (BAC). Similarly, once the initiator was added, reaction mixture gradually changed from a clear solution to a turbid emulsion, which was due to the reaction temperature (70 °C) above the LCST of the resulting copolymer. However, after polymerization, the reaction system turned transparent when cooled to room temperature, and the resulting clear polymer solution turned turbid again after heating (Figure S2). The obtained copolymer poly (VCL-*co*-MAA-3) had a low molecular weight (M_w, 1900 g/mol) and narrow molecular weight distribution (M_w/M_n, 1.02) (Figure S2), which was close to that of the oligomers composing the microgels (degraded polymer, 1400 g/mol). These results indicated that it was cross-linker that fixed the polymer network. Therefore, when the cross-linking units were broken by the reducing agents, the polymer network was disassembled into linear polymer. The results indicated that the microgels were biocompatible as the short linear polymers from disassembled microgels could be easily eliminated through the excretion pathway in vivo.

The above results supported strongly the microgels cross-linked with disulfide bonds to be responsive against reducing environment. The degradation of microgels could trigger the release of the encapsulated drugs in a reducing environment through disulfide-thiol chemistry. Thus, the multiresponsive microgels should have a great potential as drug carriers for controlled drug delivery.

DOX Loading and Release. Doxorubicin (DOX) is a DNA interacting drug widely used in chemotherapy,[49] which has also been physically entrapped into microgels.[50] To investigate the potential application of P(VCL-*s*-*s*-MAA-3)-PEG microgels as drug delivery vehicle, DOX was used as a model anticancer drug to test the loading and releasing capacity of the microgels. The P(VCL-*s*-*s*-MAA-3)-PEG microgels were loaded with DOX (1:0.3 w/w) in the DOX aqueous solution of pH 8.0 at room temperature, giving the DOX loading content of 13.8 wt % and encapsulation efficiency of 53.6%. The high drug-loading capacity resulted from the electrostatic forces and hydrogen-bond interaction between DOX and polymer.[15] The drug therapeutic effect is closely related to the release profile of the drug delivery system in the body.[51] The normal pH of blood for sustaining human life is about 7.4, while tumor tissue has a lower extracellular pH of 6.5−7.2 and drops to a pH of 5.0−5.5 when reaching the endosomes and lysosomes.[52] Therefore, meticulous investigation on drug release profile of DOX-loaded microgels was respectively conducted at 37 °C in different pHs of buffers with 150 mM NaCl. In Figure 9, 26% of DOX was released from microgels at pH 7.4 over a period of 48 h, while 54% and 75% of

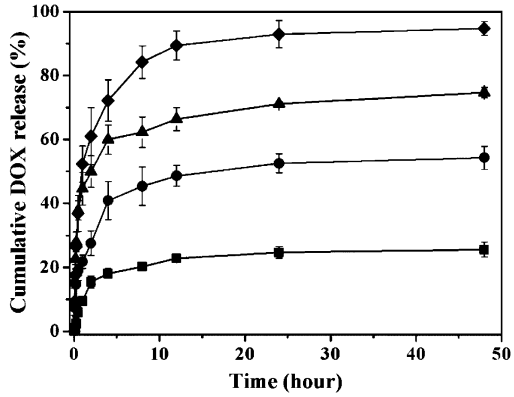

Figure 9. Stimuli-responsive DOX release profiles of DOX-loaded P(VCL-*s*-*s*-MAA-3)-PEG microgels at 37 °C in different release media with 150 mM NaCl: (■) pH 7.4, (●) pH 6.5, (▲) pH 5.5, and (♦) pH 6.5 + 10 mM GSH.

DOX was released at pH 6.5 and 5.5, respectively. The low leakage of DOX from microgels at pH 7.4 confirmed that the drug-loaded microgels could keep stable in blood circulation. The polymer network was in the swollen state at pH 7.4/37 °C due to the strong repulsion forces from carboxyl groups in higher pH condition and the higher VPTT of P(VCL-*s*-*s*-MAA-3)-PEG (41.0 °C), thereby resulting in a slow release rate. On the other hand, the enhanced electrostatic attraction between the positively charged DOX molecules and the negatively charged carboxyl groups from PMAA was unfavorable for the release of DOX molecules. However, when pH was decreased to 5.5, the polymer network was strongly collapsed as the carboxyl groups were highly protonated, and the VPTT shifted to a much lower temperature. As a consequence, the collapse of the microgels and disrupted electrostatic interaction led to a fast DOX release.

As GSH (approximately 2−10 mM) extensively existed in the cytosol and cell nucleus at a pH of 6.5−7.2 to maintain a high reducing potential,[53] we simulated the redox environment in the cytosol of mammalian cells by addition of 10 mM GSH in pH 6.5 phosphate buffer to evaluate whether the degradation of microgels in the reductive environment could trigger the drug release. As shown in Figure 9, significant acceleration of DOX release from microgels was observed in the presence of GSH in the release media. The microgels released 84% of DOX quickly within 8 h, and about 95% of DOX after 48 h. In the control experiment, 54% of DOX was released after 48 h in the absence of GSH at pH 6.5. These results indicated that DOX release could be facilitated in the intracellular reducing environment by the cleavage of disulfide bonds in the microgels.

In Vitro Cell Assays. It could be anticipated that DOX-loaded microgels would be eroded in cellular media due to the presence of 2−10 mM GSH, and, in turn, the released DOX molecules would kill cancer cells. To confirm this idea, the in vitro cell assays were used to evaluate the cellular uptake and intracellular drug release of DOX-loaded microgels and the cytotoxicity of blank microgels and DOX-loaded microgels.

Efficient cellular internalization of the nanoparticles is necessary for intracellular drug delivery and efficient therapy. To track P(VCL-*s*-*s*-MAA-3)-PEG microgels intracellularly, FITC was conjugated into the microgels by copolymerization of FITC-functionalized monomer. Confocal microscopic images

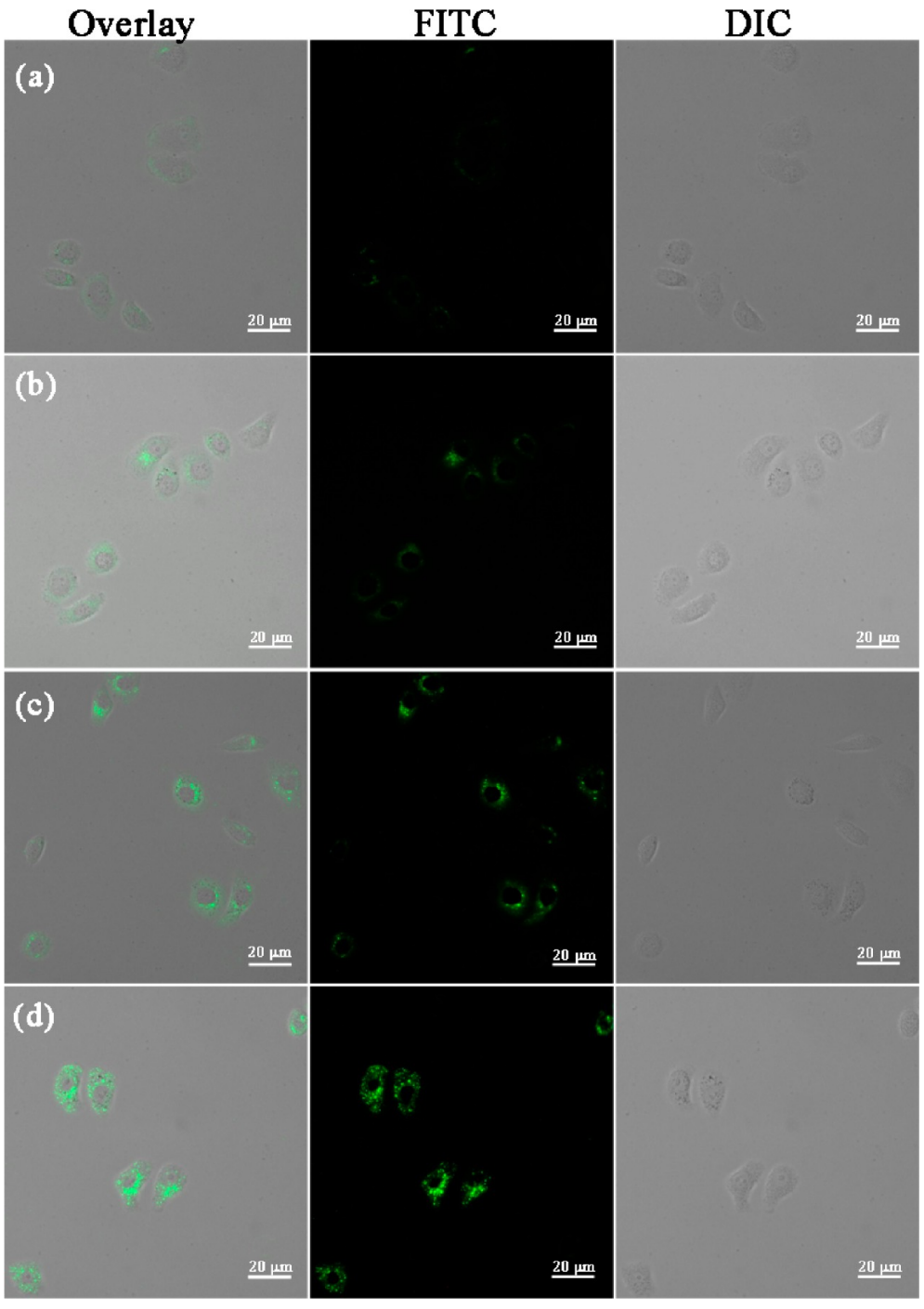

Figure 10. Confocal laser scanning microscope images of HeLa cells cultivated with blank fluorescent P(VCL-*s*-*s*-MAA-3)-PEG microgels for 0.5 h (a), 1 h (b), 2 h (c) and 4 h (d).

of HeLa cells respectively treated with the FITC-labeled particles for 0.5, 1, 2, and 4 h were captured. In Figure 10, the green fluorescent signals from FITC dye showed P(VCL-*s*-*s*-MAA-3)-PEG microgels had been internalized by HeLa cell through endocytosis or macropinocytosis.[36] As incubation time increased, the growing green fluorescent signals from FITC dye were observed, suggesting more particles were endocytized by cells with increased time.

The intracellular drug release of DOX-loaded P(VCL-*s*-*s*-MAA-3)-PEG microgels were observed by fluorescence microscopy. HeLa cells were cultured for 24 h to permit cell attachment. After 24 h, the HeLa cells were incubated with DOX-loaded microgels and free DOX at the final DOX concentration of 0.1 μg mL^{-1}. The fluorescence images of the DOX-loaded microgels were taken at predetermined intervals (2, 8, 24, and 48 h) in comparison to the free DOX and blank control. It could be shown in Figure 11 (a2) that weak DOX fluorescence was observed in the HeLa cells after 2 h incubation with DOX-loaded microgels, indicating that some microgels had been phagocytized by cells and released DOX into the cells. When the incubation time lasted for 8 and 24 h, the gradually enhanced red fluorescence was observed (Figure 11 (b2) and (c2)), which suggested that more microgels were endocytized into the cells and more DOX was released. The result of weaker red

dx.doi.org/10.1021/bm401131w | *Biomacromolecules* 2013, 14, 3034−3046

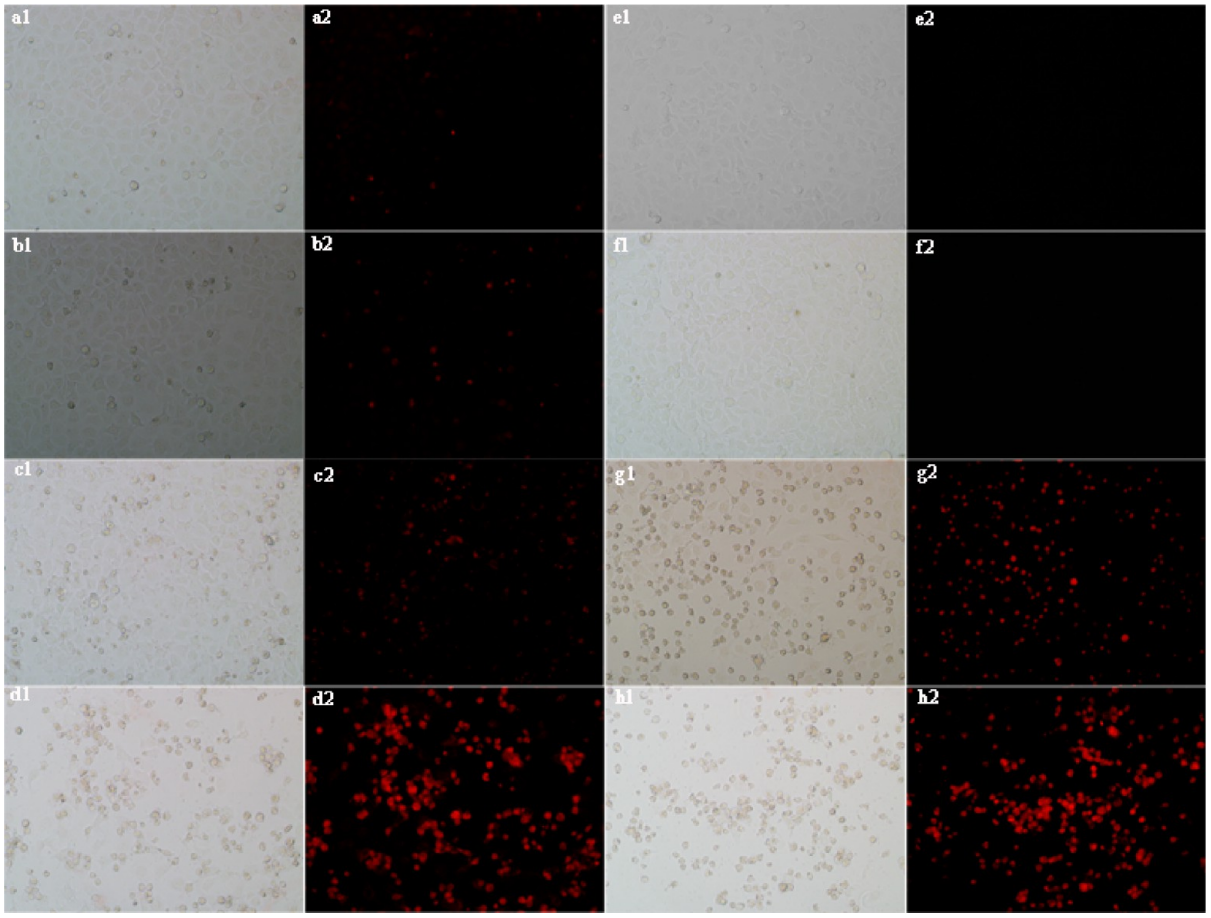

Figure 11. Phase-contrast and fluorescence images of HeLa cells upon DOX-loaded P(VCL-*s*-*s*-MAA-3)-PEG microgels over incubation: (a) 2 h, (b) 8 h, (c) 24 h and (d) 48 h; cells cultured without microgels (blank control): (e) 24 h, (f) 48 h; free DOX: (g) 24 h and (h) 48 h. 1, the DIC images; 2, fluorescence images.

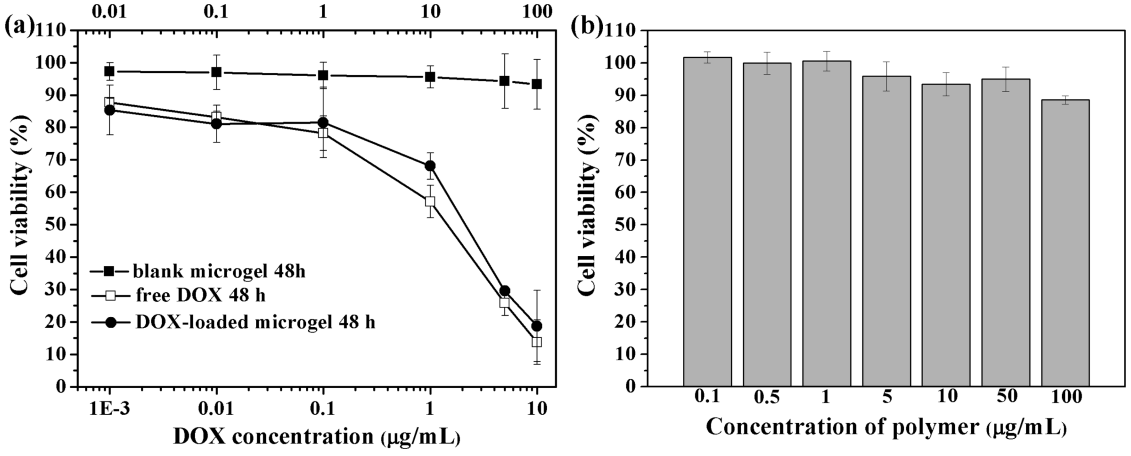

Figure 12. Cell survival assay of cells for 48 h. (a) HeLa cells: (■) blank P(VCL-*s*-*s*-MAA-3)-PEG microgels, (●) DOX-loaded P(VCL-*s*-*s*-MAA-3)-PEG microgels, and (□) free DOX. The concentration of blank microgel was shown on the top *x*-axis. (b) HK-2 cells exposed to blank P(VCL-*s*-*s*-MAA-3)-PEG microgels.

fluorescence after 24 h incubation with DOX-loaded microgels than that with free DOX (Figure 11 (g2)) correlated to the quicker diffuse rate into the cells of the free DOX[46] and the slow degradation of the microgels due to the low GSH concentration in the cells. When respective incubation with free DOX and DOX-loaded microgels lasted for 48 h, bright red fluorescence was observed in both Figure 11 (d2) and (h2). As expected, the much increased red fluorescence intensity from DOX-loaded microgels (Figure 11 (d2)) was comparable to that from free DOX (Figure 11 (h2)). These results suggested that it took a period of time for DOX-loaded microgels to release most drugs in the cells. The red fluorescence from free DOX appearing in Figure 11 (h2) was brighter than that in Figure 11 (g2), which was related to the fact that anticancer drugs could sufficiently

dx.doi.org/10.1021/bm401131w | *Biomacromolecules* 2013, 14, 3034−3046

exert the effect of killing cancer cells after 48h incubation.[54] By contrast, HeLa cells in a blank control (Figure 11 (e1) and (f1)) had a good proliferation as a control experiment.

Next, we evaluated whether the incorporation of DOX into microgels could facilitate the cytotoxic activity of the drug in HeLa cancer cells. The cytotoxicity was assessed using MTT assay against HeLa cancer cells after 48 h incubation with DOX-loaded microgels, free DOX and blank microgels, respectively. In Figure 12a, DOX-loaded microgels displayed similar cytotoxic activity to free DOX at a DOX dose of 10 μg mL^{-1}. Only 18.7% of the cells remained viable at a DOX dose of 10 μg mL^{-1} when treated with DOX-loaded microgels, while the blank microgel control showed almost no cytotoxic effect on the growth of HeLa cells. This observation illustrated that DOX-loaded P(VCL-*s*-*s*-MAA-3)-PEG microgels could efficiently kill the cancer cells due to the efficient uptake by the HeLa cells and the cumulative DOX release in the reduced intracellular microenvironment. The amount of DOX from DOX-loaded micogels required to achieve 50% of growth inhibition (IC50) for HeLa cells was 2.1 μg mL^{-1}, which was slightly higher than that of free DOX (1.4 μg mL^{-1}). To assess the cytotoxicity of P(VCL-*s*-*s*-MAA-3)-PEG microgels to normal cells, the MTT assay were also performed via 48 h incubation in normal HK-2 cell line. As shown in Figure 12b, the incubation with P(VCL-*s*-*s*-MAA-3)-PEG microgels resulted in no cytotoxicity to HK- 2 cells at the concentration range of 0.1−50 μg mL^{-1}. Furthermore, about 90% of cells were viable at the high concentration of 100 μg mL^{-1}, which was related to the excellent biocompatibility and little cytotoxicity of PVCL. Overall, the biocompatible and biodegradable nature, the capability of loading anticancer drugs, accompanied with triggered drug release in reducing intracellular microenvironment make the P(VCL-s-s-MAA-3)-PEG microgel an intriguing candidate for effective drug carriers in the tumor therapy.

CONCLUSION

In this report, a new type of temperature/pH/redox multi-responsive microgels based on PVCL was prepared via precipitation polymerization using pH-sensitive MAA and macromolecular PEGMA as comonomers, and BAC as a disulfide-linked cross-linker. The obtained microgels possessed uniform, dispersive spherical shape with the average hydrodynamic diameter smaller than 300 nm and narrow size distribution (PI < 0.1). These microgels underwent adjustable volume phase transition affected not only by the amount of MAA incorporated but also by the changing of pH. The P(VCL-*s*-*s*-MAA-3)-PEG microgel, which had excellent stability and the appropriate VPTT in physiological condition, could be eroded in reductive environment due to the cleavage of the disulfide linkages. Moreover, P(VCL-*s*-*s*-MAA-3)-PEG microgel could effectively encapsulate DOX inside with drug load content up to 13.8% due to the electrostatic forces and hydrogen-bond interaction between DOX and polymer. The drug release profiles indicated low leakage of DOX from microgels at pH 7.4 and rapid release from the microgels in acidic and reducing condition. The cytotoxicity assay against normal HK-2 cells indicated the microgels were nontoxic and biocompatible. Cytotoxicity of the DOX-loaded microgels against HeLa cells, the cellular uptake of the microgels and intracellular release behavior of DOX demonstrated that the microgels could be internalized by HeLa cell and kill the cells effectively. These results suggested that the biodegradable P(VCL-*s*-*s*-MAA-3)-PEG microgels, with temperature/pH/redox multiple sensitivity, could be used to construct safe and promising drug delivery systems for targeting cancer therapy.

ASSOCIATED CONTENT

Supporting Information

Table of the reproducibility recipes and colloidal data of microgels; ^{1}H NMR spectrum of VCL in D_2O and ^{1}H NMR spectra corresponding to the samples withdrawn in the reaction of P(VCL-s-s-MAA-3) at different reaction times; and the molecular weight of copolymer poly(VCL-*co*-MAA) by GPC measurement and the appearance of the resulting copolymer at low temperature and high temperature. This material is available free of charge via the Internet at http://pubs.acs.org.

AUTHOR INFORMATION

Corresponding Author

*Mailing address: State Key Laboratory of Molecular Engineering of Polymers and Department of Macromolecular Science, Fudan University, No.220 Handan Road, Shanghai, 200433 China. Tel: +86 21 6564 2385. Fax: +86 21 6564 0293. E-mail: wlyang@fudan.edu.cn.

Notes

The authors declare no competing financial interest.

ACKNOWLEDGMENTS

We are grateful for the support of the National Science Foundation of China (Grant No. 20874015 and 51273047), the Shanghai Rising-Star Program (10QH1400200), and the "Shu Guang" project (12SG07) supported by Shanghai Municipal Education Commission and Shanghai Education Development Foundation.

REFERENCES

(1) Azzopardi, E. A.; Ferguson, E. L.; Thomas, D. W. *J. Antimicrob. Chemother.* **2013**, *68*, 257−274.
(2) Elsabahy, M.; Wooley, K. L. *Chem. Soc. Rev.* **2012**, *41*, 2545−2561.
(3) Matsumura, Y.; Maeda, H. *Cancer Res.* **1986**, *46*, 6387−6392.
(4) Petros, R. A.; DeSimone, J. M. *Nat. Rev. Drug Discovery* **2010**, *9*, 615−627.
(5) Klinger, D.; Landfester, K. *Polymer* **2012**, *53*, 5209−5231.
(6) Oh, J. K.; Siegwart, D. J.; Lee, H. I.; Sherwood, G.; Peteanu, L.; Hollinger, J. O.; Kataoka, K.; Matyjaszewski, K. *J. Am. Chem. Soc.* **2007**, *129*, 5939−5945.
(7) Bhuchar, N.; Sunasee, R.; Ishihara, K.; Thundat, T.; Narain, R. *Bioconjugate Chem.* **2012**, *23*, 75−83.
(8) Boyko, V.; Richter, S.; Grillo, I.; Geissler, E. *Macromolecules* **2005**, *38*, 5266−5270.
(9) Das, M.; Mardyani, S.; Chan, W. C. W.; Kumacheva, E. *Adv. Mater.* **2006**, *18*, 80−83.
(10) Imaz, A.; Forcada, J. *J. Polym. Sci., Part A: Polym. Chem.* **2011**, *49*, 3218−3227.
(11) Pich, A.; Tessier, A.; Boyko, V.; Lu, Y.; Adler, H. J. P. *Macromolecules* **2006**, *39*, 7701−7707.
(12) Beija, M.; Marty, J.-D.; Destarac, M. *Chem. Commun.* **2011**, *47*, 2826−2828.
(13) Cavus, S.; Cakal, E. *Ind. Eng. Chem. Res.* **2012**, *51*, 1218−1226.
(14) Imaz, A.; Forcada, J. *Macromol. Symp.* **2009**, *281*, 85−88.
(15) Imaz, A.; Forcada, J. *J. Polym. Sci., Part A: Polym. Chem.* **2010**, *48*, 1173−1181.
(16) Koniger, A.; Plack, N.; Kohler, W.; Siebenburger, M.; Ballauff, M. *Soft Matter* **2013**, *9*, 1418−1421.
(17) Pelton, R. H.; Chibante, P. *Colloids Surf.* **1986**, *20*, 247−256.
(18) Qiu, Y.; Park, K. *Adv. Drug Delivery Rev.* **2001**, *53*, 321−339.
(19) Vihola, H.; Laukkanen, A.; Valtola, L.; Tenhu, H.; Hirvonen, J. *Biomaterials* **2005**, *26*, 3055−3064.

(20) Ramos, J.; Imaz, A.; Forcada, J. *Polym. Chem.* **2012**, *3*, 852−856.
(21) Bulmus, V.; Chan, Y.; Nguyen, Q.; Tran, H. L. *Macromol. Biosci.* **2007**, *7*, 446−455.
(22) Ercole, F.; Thissen, H.; Tsang, K.; Evans, R. A.; Forsythe, J. S. *Macromolecules* **2012**, *45*, 8387−8400.
(23) Klinger, D.; Landfester, K. *Macromolecules* **2011**, *44*, 9758−9772.
(24) Cheng, R.; Feng, F.; Meng, F. H.; Deng, C.; Feijen, J.; Zhong, Z. Y. *J. Controlled Release* **2011**, *152*, 2−12.
(25) Schafer, F. Q.; Buettner, G. R. *Free Radical Biol. Med.* **2001**, *30*, 1191−1212.
(26) Sivakumar, S.; Bansal, V.; Cortez, C.; Chong, S. F.; Zelikin, A. N.; Caruso, F. *Adv. Mater.* **2009**, *21*, 1820−1824.
(27) Groll, J.; Singh, S.; Albrecht, K.; Moeller, M. *J. Polym. Sci., Part A: Polym. Chem.* **2009**, *47*, 5543−5549.
(28) Nayak, S.; Lyon, L. A. *Angew. Chem., Int. Ed.* **2005**, *44*, 7686−7708.
(29) Imaz, A.; Miranda, J. I.; Ramos, J.; Forcada, J. *Eur. Polym. J.* **2008**, *44*, 4002−4011.
(30) Chu, B.; Wang, Z. L.; Yu, J. Q. *Macromolecules* **1991**, *24*, 6832−6838.
(31) Makhaeva, E. E.; Tenhu, H.; Khokhlov, A. R. *Macromolecules* **2002**, *35*, 1870−1876.
(32) Saunders, B. R.; Vincent, B. *Adv. Colloid Interface Sci.* **1999**, *80*, 1−25.
(33) Varga, I.; Gilanyi, T.; Meszaros, R.; Filipcsei, G.; Zrinyi, M. *J. Phys. Chem. B* **2001**, *105*, 9071−9076.
(34) Shah, S.; Pal, A.; Gude, R.; Devi, S. *Eur. Polym. J.* **2010**, *46*, 958−967.
(35) Yuan, L.; Chen, W. L.; Li, J.; Hu, J. H.; Yan, J. J.; Yang, D. *J. Polym. Sci., Part A: Polym. Chem.* **2012**, *50*, 4579−4588.
(36) Dai, J.; Lin, S. D.; Cheng, D.; Zou, S. Y.; Shuai, X. T. *Angew. Chem., Int. Ed.* **2011**, *50*, 9404−9408.
(37) Imaz, A.; Forcada, J. *J. Polym. Sci., Part A: Polym. Chem.* **2008**, *46*, 2510−2524.
(38) Pelton, R. H.; Pelton, H. M.; Morphesis, A.; Rowell, R. L. *Langmuir* **1989**, *5*, 816−818.
(39) Meeussen, F.; Nies, E.; Berghmans, H.; Verbrugghe, S.; Goethals, E.; Du Prez, F. *Polymer* **2000**, *41*, 8597−8602.
(40) Pohlmeier, A.; Haber-Pohlmeier, S. *J. Colloid Interface Sci.* **2004**, *273*, 369−380.
(41) Hoare, T.; Pelton, R. *Langmuir* **2004**, *20*, 2123−2133.
(42) Wong, J. E.; Diez-Pascual, A. M.; Richtering, W. *Macromolecules* **2009**, *42*, 1229−1238.
(43) Kratz, K.; Hellweg, T.; Eimer, W. *Colloids Surf. A: Physicochem. Eng. Aspects* **2000**, *170*, 137−149.
(44) Chang, B. S.; Sha, X. Y.; Guo, J.; Jiao, Y. F.; Wang, C. C.; Yang, W. L. *J. Mater. Chem.* **2011**, *21*, 9239−9247.
(45) Pich, A.; Berger, S.; Ornatsky, O.; Baranov, V.; Winnik, M. A. *Colloid Polym. Sci.* **2009**, *287*, 269−275.
(46) Prabaharan, M.; Grailer, J. J.; Pilla, S.; Steeber, D. A.; Gong, S. Q. *Biomaterials* **2009**, *30*, 3009−3019.
(47) Meng, F. H.; Hennink, W. E.; Zhong, Z. *Biomaterials* **2009**, *30*, 2180−2198.
(48) Gaulding, J. C.; Smith, M. H.; Hyatt, J. S.; Fernandez-Nieves, A.; Lyon, L. A. *Macromolecules* **2012**, *45*, 39−45.
(49) Unverferth, D. V.; Magorien, R. D.; Leier, C. V.; Balcerzak, S. P. *Cancer Treat. Rev.* **1982**, *9*, 149−164.
(50) Missirlis, D.; Tirelli, N.; Hubbell, J. A. *Langmuir* **2005**, *21*, 2605−2613.
(51) Hubbell, J. A.; Chilkoti, A. *Science* **2012**, *337*, 303−305.
(52) Duncan, R. *Nat. Rev. Drug Discovery* **2003**, *2*, 347−360.
(53) Casey, J. R.; Grinstein, S.; Orlowski, J. *Nat. Rev. Mol. Cell Biol.* **2010**, *11*, 50−61.
(54) Wang, P. W.; Henning, S. M.; Heber, D. *PLoS One* **2010**, *5*, 1191−1212.